ACS OMEGA

http://pubs.acs.org/journal/acsodf

Article

Magnetic Nanoparticle Coating Decreases the Senescence and Increases the Targeting Potential of Fibroblasts and Adipose-Derived Mesenchymal Stem Cells

Camelia-Mihaela Zară-Dănceanu,[⊥] Anca-Emanuela Minuti,[⊥] Cristina Stavilă, Luminiţa Lăbuscă,* Dumitru-Daniel Herea,* Crina Elena Tiron, Horia Chiriac, and Nicoleta Lupu

Cite This: *ACS Omega* 2023, 8, 23953−23963

Read Online

ACCESS | Metrics & More | Article Recommendations | Supporting Information

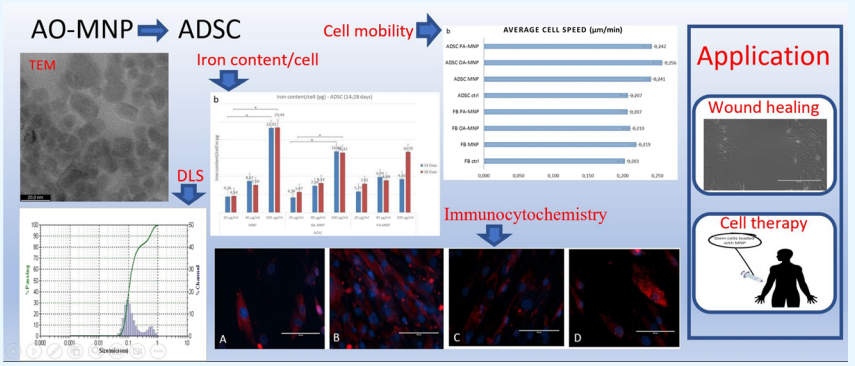

ABSTRACT: Magnetic nanoparticles (MNPs) are intensely scrutinized for applications in emerging biomedical fields. Their potential use for drug delivery, tracking, and targeting agents or for cell handling is tested for regenerative medicine and tissue engineering applications. The large majority of MNPs tested for biomedical use are coated with different lipids and natural or synthetic polymers in order to decrease their degradation process and to increase the ability to transport drugs or bioactive molecules. Our previous studies highlighted the fact that the as-prepared MNP-loaded cells can display increased resistance to culture-induced senescence as well as ability to target pathological tissues; however, this effect tends to be dependent on the cell type. Here, we assessed comparatively the effect of two types of commonly used lipid coatings, oleic acid (OA) and palmitic acid (PA), on normal human dermal fibroblasts and adipose-derived mesenchymal cells with culture-induced senescence and cell motility in vitro. OA and PA coatings improved MNPs stability and dispersibility. We found good viability for cells loaded with all types of MNPs; however, a significant increase was obtained with the as-prepared MNPs and OA-MNPs. The coating decreases iron uptake in both cell types. Fibroblasts (Fb) integrate MNPs at a slower rate compared to adipose-derived mesenchymal stem cells (ADSCs). The as-prepared MNPs induced a significant decrease in beta-galactosidase (B-Gal) activity with a nonsignificant one observed for OA-MNPs and PA-MNPs in ADSCs and Fb. The as-prepared MNPs significantly decrease senescence-associated B-Gal enzymatic activity in ADSCs but not in Fb. Remarkably, a significant increase in cell mobility could be detected in ADSCs loaded with OA-MNPscompared to controls. The OA-MNPs uptake significantly increases ADSCs mobility in a wound healing model in vitro compared to nonloaded counterparts, while these observations need to be validated in vivo. The present findings provide evidence that support applications of OA-MNPs in wound healing and cell therapy involving reparative processes as well as organ and tissue targeting.

INTRODUCTION

Magnetic nanomaterials and particularly magnetic nanoparticles (MNPs) are intensively scrutinized as effective tools in nanobiology and nanomedicine. Due to their versatility and magnetic responsiveness, MNPs are currently tested for applications such as drug delivery,[1] cell tracking or targeting for cell therapy and regenerative medicine applications,[2] and tissue engineering of bones,[3] cartilage,[4] blood vessels,[5] or other complex tissues that require a controlled assembly.[6] MNPs are investigated as potential adjuvant therapy in solid malignancies due to their ability to function as seeds for the delivery of local hyperthermia.[7]

Received: April 12, 2023
Accepted: June 9, 2023
Published: June 22, 2023

https://doi.org/10.1021/acsomega.3c02449
ACS Omega 2023, 8, 23953−23963

The main advantages of using MNPs compared to other nanoparticles include their magnetic responsiveness as well as good biocompatibility. The availability of enzymatic equipment for handling metabolites is one of the main prerequisites for nano- and biomaterial biocompatibility. Iron-based MNPs are shown to be degraded by means of cell- and cell status-dependent molecular pathways involved in iron transport and storage.[8]

It is to be mentioned, however, that MNPs physical and chemical characteristics such as size, shape, electric charge, and coating are important predictors of their interaction at the cell and tissue levels. MNPs possess high surface energy, a fact that imposes some limitations for their use as they tend to spontaneously form aggregates. Various coating procedures are required for better stability in aqueous solution. The cell type and phenotype are other significant parameters that influence their interaction with MNPs. It has been reported that the as-prepared iron nanoparticles can form reactive oxygen species, which introduce dose-dependent cell and tissue toxicity. To circumvent these problems, MNPs cores can be coated with organic or inorganic compounds, surfactants (oleic acid, lauric acid, etc.), and artificial or natural polymers.[9]

For delivery purposes, it is common practice to employ coatings that bond to MNPs cores and at the same time allow for targeted or on-demand delivery of the ferried drug or bioactive molecule.[10] Stem cells have been proposed as a modality to facilitate the transport of MNPs with or without a pharmacological payload for the purpose of targeted tumor treatment or regenerative medicine applications in cell therapy or tissue engineering.[11]

We previously reported on the remarkable ability of uncoated MNPs (Fe_3O_4) to delay culture-induced senescence in adipose-derived mesenchymal cells (ADSCs) as well as on the increased ability of MNP-loaded ADSCs to target tumor-like tissues in vitro.[12] Coating iron oxide particles with various polymers is required for transferability as well as the manufacturing perspective.

In this study, we compared the effect of the coating type on the MNPs interaction with two cell types, aiming to detect the best cell−particle combination that could be used for avoiding culture-induced senescence as well as for increasing cell mobility when used for therapeutic purposes. Mesenchymal cell progenitors human ADSCs and human normal dermal fibroblast (Fb) primary cells were tested, focusing on the particle upload, effect on culture-induced senescence, and cell migratory ability investigated at the protein level. Two types of coatings, oleic acid and palmitic acid (sodium palmitate), were tested against the use of the as-prepared, noncoated proprietary iron oxide MNPs.

MATERIALS AND METHODS

MNP Preparation and Coating. Magnetic nanoparticles (Fe_3O_4) were prepared using the chemical coprecipitation method. Thus, 3.3 g of $FeCl_2{\cdot}4H_2O$ was dissolved in 10 mL of ultrapure water, then filtered, and mixed with 12 mL of $FeCl_3{\cdot}6H_2O$ (45% - w/v). The obtained solution was immediately added in 1.2 L of ultrapure water under mechanical stirring (800 rpm). Then, 100 mL of NaOH solution (15%) was added, and the color of the solution quickly turned black. After 2 min, the heating was stopped, and the stirring was stopped after 70 min. MNPs were magnetically separated and washed until the pH of the solution reached 6.5. For coating with oleic acid (OA), 200 μL of OA was added over an appropriate amount of uncoated magnetite and subjected to ultrasonication for 30 min. The resulting oleic acid-coated magnetite nanoparticles were washed several times with deionized water to pH ±7. For coating with palmitic acid (PA), 0.2 g of PA was dissolved in 50 mL of acetone (45−50 °C). 20 mL of deionized water and 4.5 g of NaOH were added to this solution under mechanical stirring (700 rpm). The temperature was then increased to 95−100 °C, and 30 mL of deionized water was immediately added. After boiling the solution, to evaporate the acetone, deionized water was added to attain 100 mL of the final solution. The final solution was clear and kept at 90−100 °C until use. Separately, 5 g of $FeCl_3{\cdot}6H_2O$ was dissolved in 200 mL of deionized water under heating at 80 °C, followed by the addition of 1.9 g of $FeCl_2{\cdot}4H_2O$ and 2 mL of acetic acid. The temperature was increased to 95 °C, and the heated sodium palmitate/sodium hydroxide solution prepared previously was slowly poured over the salt solution with vigorous stirring. Once the color of the solution turned black, the heating was stopped and stirring was continued for another 1 h, and it was further washed until reaching pH 6.5−7.

MNP Characterization. MNPs were characterized in terms of size by using a dynamic light scattering method (DLS-Microtrac/Nanotrac 252, Montgomeryville) and ultra-high-resolution transmission electron microscopy imaging (Libra200 UHR-TEM, Carl Zeiss, Germany). Magnetization was evaluated by using a vibrating sample magnetometer (VSM) (LakeShore 7410), while the composition was characterized through a Bruker AXS D8-Advance powder X-ray diffractometer (Cu Kα radiation, k = 0.1541 nm). Fourier transform infrared spectroscopy (FTIR) measurement was carried out with a Fourier transform infrared spectrometer, FTIR JASCO 6100.

Primary Adipose-Derived Mesenchymal Cells and Human Dermal Fibroblasts. We utilized primary adipose-derived mesenchymal cells obtained from fresh lipoaspirate from donors undergoing elective liposuction procedures after ethical board approval and informed donor consent. ADSCs extraction was performed as previously described.[12] Briefly, lipoaspirate was washed with sterile phosphate-buffered saline (PBS) with 2% antibiotic, treated with 0.1% collagenase (collagenase type I Sigma Aldrich), incubated at 37 °C for 2−3 h, filtered using a 100 μm cell strainer, and centrifuged at 300g for 5 min. Pellets resuspended in complete culture medium (CCM) (DMEM with 10% FBS and 2% antibiotic) were plated in size-appropriate culture flasks. Cells at passages 2−3 were used for experiments in this study. For obtaining dermal fibroblasts, pieces of dermal tissue obtained from removed skin pieces from patients undergoing scar revision were processed as previously described.[13,14] Briefly, skin pieces were carefully washed with PBS plus 2% antibiotic, and the skin layer was scraped to remove keratinocytes and cut into square pieces of 0.5 mm and placed inside Petri dishes of 36.5 mm in CCM. After 5−7 days, fibroblasts were retrieved by trypsinization to separate from keratinocytes and further expanded.

MNP Cytotoxicity/Cell Viability. For cytotoxicity, ADSCs and Fb in passages 2−3 were plated in 96-well plates, at 1×10^4 cells/well, and incubated for 48 h. MNPs, OA-MNPs, and PA-MNPs of 20, 40, 80, and 100 μg/mL were added to cell culture media after 48 h, each sample in triplicate. The 5-dimethylthiazol-2-yl-2,5-diphenyltetrazolium bromide (MTT) test (Vybrant MTT cell proliferation assay TermoFisher Scientific) was performed according to the manufacturer's instructions with dimethylsulfoxide (DMSO) as a dilution agent. Cell viability (CV) was calculated using the formula CV = 100 × (ODs − ODb)/(ODc − ODb), ODs = particle-treated cell OD; ODb = blank (media only) OD; and ODc = untreated

https://doi.org/10.1021/acsomega.3c02449
ACS Omega 2023, 8, 23953−23963

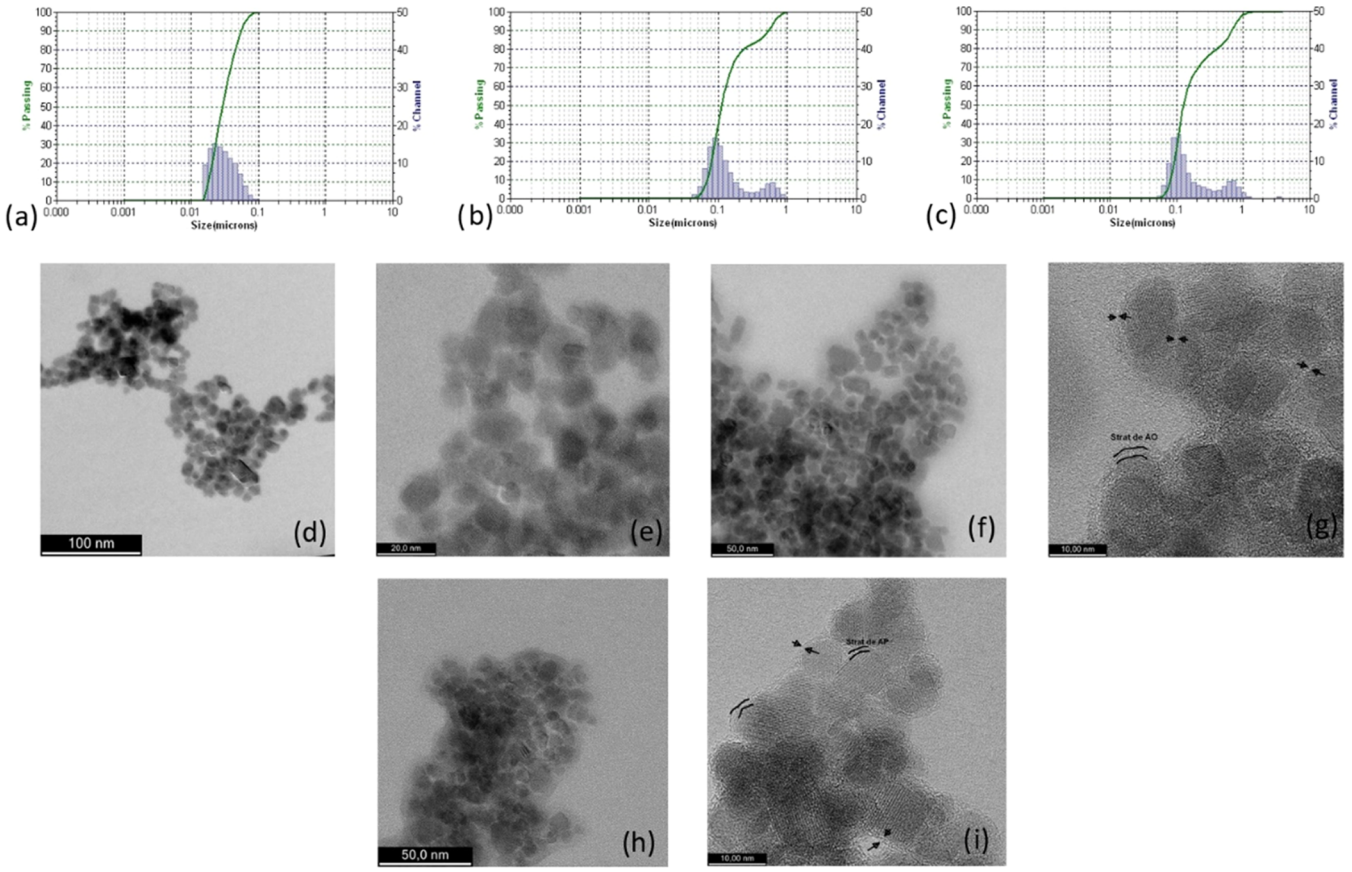

Figure 1. Dynamic light scattering and ultrahigh-resolution transmission electron microscopy (UHR-TEM) images of magnetic nanoparticles: (a) DLS for the as-prepared MNPs, (b) DLS for OA-MNPs, (c) DLS for PA-MNPs; (d, e) TEM images for the as-prepared MNPs; (f, g) TEM for OA-MNPs, and (h, i) TEM for PA-MNPs.

cell optical density (OD). For extended long-term viability, a similar protocol was used for the MTT test on cells at 48 h, 4 days, and 7 days after introduction of MNPs in the culture media. Absorbance was measured at 570 nm (Synergy HTX Multi-Mode Reader-Bioteck).

Quantitative Assessment of MNP Upload by ADSC-Ferrozine Assay. ADSCs and Fb were plated in 24-well plates at 1×10^5 cells/well. After 24 h, bare MNPs, OA-MNPs, and PA-MNPs were added. At 2, 5, 7, and 10 days, cells were double-washed with PBS to remove any extracellular MNPs. They were fixed in 70% ethanol for 15 min and double-washed with PBS. 500 μL of 50 mM NaOH was added to three wells per experiment for 2 h on a shaking plate. Aliquots of cell lysates were then transferred to 1.5 mL Eppendorf tubes and mixed with 500 μL of 10 mM HCl and 500 μL of iron-releasing reagent (a freshly mixed solution of equal volumes of 1.4 M HCl) and 4.5% (w/v) $KMnO_4$ (Merck, Germany) in distilled H_2O. These mixtures were incubated for 2 h at 60 °C within a fume hood. 150 μL of iron-detection reagent (6.5 mM ferrozine (Sigma-Aldrich, St. Louis), 6.5 mM neocuproine (Sigma-Aldrich), 2.5 M ammonium acetate, and 1 M ascorbic acid (Sigma-Aldrich) dissolved in water) were added to each tube. After 30 min, 500 μL of the solution was transferred into a well of a 24-well plate, and the absorbance was read at 570 nm. A calibration curve was set up using $FeCl_3$ standards (0−300 μM) in 10 mM HCl. The remaining two wells were stained with diamidino-2-phenylindole (DAPI TermoFisher Scientific) at 0.1 μg/mL for 5 min and washed twice. Cell count/well (x) was characterized using a fluorescent microscope and a grid using the formula $x = 2 \times A/(L \times L) \times N$, where A is the surface of the well, L is the size of one square in the grid, and N is the number of cells per region of interest (ROI). The cell count for at least five ROI was averaged per sample.

Beta-Galactosidase Assay (Fluorometric). MNP-loaded and nonloaded ADSCs were seeded in 24-well plates at 4×10^5 cells/well. Beta-galactosidase enzyme activity was quantified using a beta-galactosidase (B-Gal) detection kit (Fluorometric) (Abcam) as per the manufacturer's instructions. Briefly, cells at 14 and 28 days of culture were lysed using four cycles of frost−defrost followed by addition of the fluorescein di-β-D-galactopyranoside (FDG) stock solution followed by 1 h of incubation at 37 °C and stop buffer solution and read with a microplate reader (490−550 nm excitation/emission). The cell number was calculated at each time point as described for the ferrozine assay.

Beta-Galactosidase and CXCR4 Assay (Immunocytochemistry (ICC)). For ICC tests, 1×10^5 cells were seeded in 24-well plates. The as-prepared and coated MNPs were added after 48 h (40 μg/mL). After 14 days, cells were fixed with methanol or 4% paraformaldehyde (PFA). For beta-galactosidase detection, cells were permeabilized with 0.1% Triton X-100, blocked with 10% serum (45 min at 25 °C), and incubated with the beta-galactosidase antibody (Product #PA5-102503) (1:200, 1 h, 37 °C), followed by goat anti-rabbit Ig G Alexa Fluor 594 at a dilution of 1:600. For CXCR4 detection, methanol-fixed cells were permeabilized with 0.1% Triton X-100 for 5−10 min and blocked with 3% BSA-PBS for 30 min at RT. Cells were treated with the CXCR4 antibody (# PA3-305 Thermo Fisher) in 3%

https://doi.org/10.1021/acsomega.3c02449
ACS Omega 2023, 8, 23953−23963

BSA-PBS at a dilution of 1:100 and incubated overnight at 4 °C. Cells were washed with PBS and incubated with a secondary antibody for 1 h at RT. For detection of both ab, in the final step, 20 μL of 4′,6-diamidino-2-phenylindole (DAPI) in 200 μL of PBS was added and imaged with a fluorescent microscope.

Western Blot (WB). For WB tests, cells were cultured in T75 culture dishes and seeded at 5×10^5 density until 85% confluence. MNPs, OA-MNPs, and PA-MNPs were added after at least 48 h in culture. Whole cell pellets were lysed using 4× Laemmli buffer with mixed protease inhibitor solution. Protein concentrations were determined using the Quick Start Bradford Protein Assay Kit 1 (5000201, Bio-Rad Laboratories) according to the manufacturer's instructions. 40 μg of proteins was separated by electrophoresis on 8 and 10% sodium dodecyl sulfate (SDS)−poly(acrylamide) gradient gels and transferred to poly(vinylidene fluoride) (PVDF) membranes. Furthermore, the membranes were incubated with specific antibodies, beta-galactosidase antibody (1:500, PA5-102503, Thermo Fisher Scientific) and CXCR4 polyclonal antibody (1:500, PA5-105597, Thermo Fisher Scientific), and the blots were incubated at 4 °C overnight with shaking. Afterward, membranes after washing three times with TBST were incubated with goat anti-rabbit Ig G (H + L) (G21234, Thermo Fisher Scientific)-linked secondary antibodies (1:1000) for 1 h at room temperature. The proteins were visualized using Clarity Western ECL Substrate (1705061, BioRad) and Image Studio Digits software provided by Li-Cor (Lincoln, Nebraska).

In Vitro Wound Healing Model. 2×10^5 cells were seeded in Petri dishes. MNPs, OA-MNPs, and PA-MNPs were added after cell confluence (24−48 h). After 24 h of cell/particle interaction, a "wound" of approx. 1−1.5 mm was inflicted in the middle of the Petri dish using a cell scraper. Cells were placed within a mini-incubator and observed using time lapse microscopy for 24 h under a fluorescent inverted microscope. Individual cell elements were traced, and the distance traveled between the "wound edges" was calculated. Images were taken at intervals of 10 min for up to 24 h and processed using image analysis software (Digimizer).

RESULTS AND DISCUSSION

MNP Characterization. *Dynamic Light Scattering.* The average diameter of magnetic nanoparticles increased from 29.4 nm (PDI = 0.38) for the as-prepared MNPs (Figure 1a) to 100 nm (PDI = 0.194) for OA-coated MNPs (Figure 1) and 112 nm (PDI = 0.311) for PA-coated MNPs (Figure 1c). This increase is produced by the additional lipid layer as well as by their tendency to form clusters. DLS revealed that Fe_3O_4 nanoparticles coated with oleic acid and palmitic acid tend to organize in clusters ranging from 60 to 112 nm. Additionally, the ζ-potential (ZP) is displayed for both formulations (Table 1), indicating high stabilization of the AO-MNP and AP-MNP. The current data are in accordance with the literature; solutions with ZP higher than +20 or lower than −20 mV are considered stable.

Transmission Electron Microscopy. UHR-TEM images reveal that the as-prepared MNP has a very homogeneous structure, with diameters very close to 20 nm. There is a tendency for uncoated nanoparticles to agglomerate (Figure 1d,e), a fact that further justifies the necessity for coating when considered for biological applications. The coating layer of oleic acid and palmitic acid with a thickness of 1−2 nm is highlighted in Figure 1g,f. As expected, OA- and PA-coated MNPs agglomerate less compared to the as-prepared MNPs (Figure 1g,e).

Table 1. DLS Data Listing Mean Diameter, Polydispersity Index (PDI), and ζ-Potential (ZP) of MNPs Formulations

MNP formulation	physical characterization	
as-prepared MNP	mean diameter (nm)	29.4
	PDI	0.38
	ZP	0.49
AO-MNP	mean diameter (nm)	100
	PDI	0.194
	ZP	0.82
AP-MNP	mean diameter (nm)	112
	PDI	0.311
	ZP	0.68

X-ray Diffraction. X-ray diffraction highlights the crystalline nature of MNPs. Figure 2 a shows the X-ray diffractograms for the three types of magnetic particles evaluated: as-prepared MNPs (orange line), palmitic acid-coated MNPs (red line), and oleic acid-coated MNPs (violet line in the graph). X-ray diffraction (XRD) analysis revealed the presence of two crystalline phases Fe_3O_4 (magnetite) and γ-Fe_2O_3 (maghemite), with an orthorhombic structure. The general appearance of the diffraction planes reflects the crystalline character of the sample and small crystallite sizes (10−12 nm), with possible particle agglomerations.

Magnetic properties of Fe_3O_4 MNPs, OA-MNPs, and PA-MNPs were characterized. Hysteresis cycles (Figure 2b) were measured in magnetic fields between −20 and 20 kOe at room temperature. The as-prepared MNPs saturation magnetization was 64.013 emu/g (red line), while for those coated with oleic acid and palmitic acid, it slightly decreases to 57.626 (blue line) and 60.389 emu/g (red line within the graph), respectively.

The remanent magnetization of the as-prepared MNPs was found to be higher than that of those coated with oleic acid and palmitic acid, respectively. The difference between the two types of particles, coated and uncoated, is indirect evidence of the binding of nonmagnetic fatty acids to the surface of the nanoparticles. MNPs coated with palmitic and oleic acids display lower coercivity values, being closer to a superparamagnetic behavior, which makes them less susceptible to agglomeration.

FTIR Spectra. The FTIR spectra of Fe_3O_4 magnetic nanoparticles show sharp bands in the range of 440−444 and 560−590 cm^{-1} attributed to the intrinsic stretching vibrations of oxygen in the metal bonds, corresponding to the tetrahedral and octahedral coordination, respectively, characteristics of the spinel-type structure. Moreover, several bands are detected in the range of 3439−1383 cm^{-1}, which correspond to the vibration mode of the surfactant. The vibrational bands, characteristic of the COO^- group, in the spectrum are highlighted in the range of 1387−1622 cm^{-1} and can be attributed to the asymmetric and symmetric (COO^-) stretching vibrations. The bands appearing at 3400, 2923−2927, and 2850−2846 cm^{-1} are related to the bond stretching of the hydrophilic OH group and the hydrophobic CH_2 group (Figure 2c). These bands confirm the presence of the surfactant on the surface of nanoparticles. The presence of both hydrophilic and hydrophobic groups on the surface of nanoparticles presents a series of advantages, including an increase in colloidal stability. This feature facilitates further extra functionalization with macromolecular compounds for biomedical applications.

Cell Viability. As assessed using MTT assay, excellent cell viability was detected with increasing doses of MNPs, PA-

https://doi.org/10.1021/acsomega.3c02449
ACS Omega 2023, 8, 23953−23963

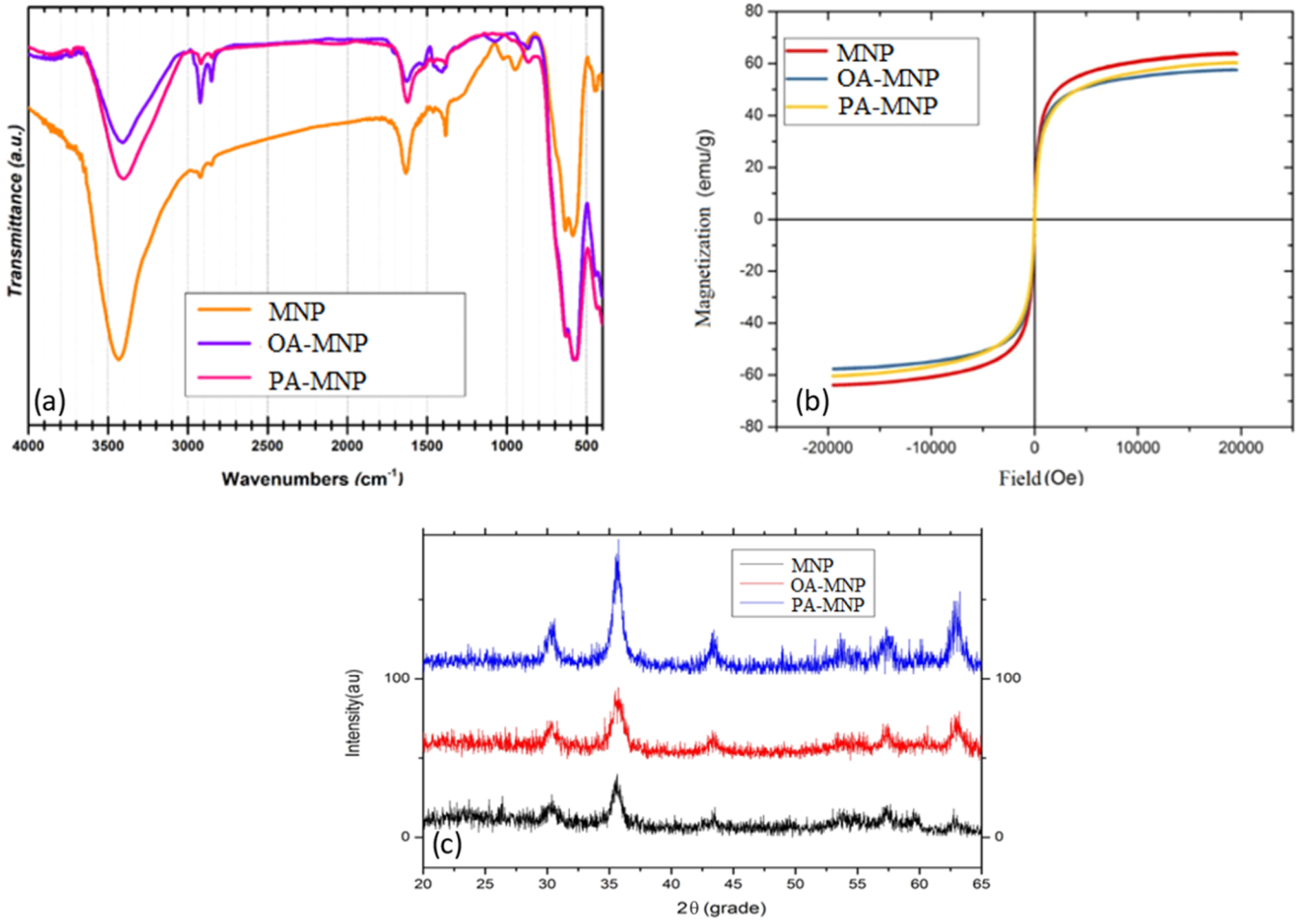

Figure 2. (a) FTIR spectra of the as-prepared MNPs (orange line), OA-MNPs (purple line), and PA-MNPs (pink line); (b) magnetization loop of the as-prepared MNPs (red line), OA-MNPs (blue line), PA-MNPs (yellow line); and (c) XRD pattern of the as-prepared MNPs (black line), OA-MNPs (red-line), and PA-MNPs (blue line).

MNPs, and OA-MNPs (20, 40, 80, and 100 μg/mL) for both ADSCs and Fb. After 48 h of cell−particle interaction, viability with PA-MNPs was slightly, nonsignificantly, lower compared to that of MNPs and OA-MNPs (Figure 3a); however, it did not decrease below 107% compared to that of nontreated cells (Fb). At 4 days, PA-MNPs-treated Fb and ADSCs decreased to the lowest of 95.81% (Fb) and 109.3% (ADSCs), respectively, recovering at 7 days (Figure 3b,c). Remarkably, the highest viability at all time points, significantly higher for ADSCs as well as for Fb, was obtained from MNPs- and OA-MNP-treated cells in the highest concentration used (100 μg/mL). The increase in viability persisted over time, up to 7 days; especially in MNPs- and OA-MNP-loaded cells, signaling increased the proliferation rate.

Indeed, based on the cell count performed for other tests (see below), the highest proliferation rate as expressed by calculated population doubling was detected for ADSCs and Fb treated with 100 μg/mL MNPs and OA-MNPs (Supporting Information, Figure 1). At 7 days, ADSC-MNPs, OA-MNPs, and PA-MNPs viability was significantly higher compared to controls for the case of 100 μg/mL added to culture media.

The iron cellular content and iron upload were characterized. The iron cellular content was calculated based on spectrophotometric detection of iron in cell lysates normalized to the iron content of nonloaded counterparts, relative to the cell number (ferrozine assay). As expected, the amount of iron per cell acquired within a maximum of 28 days after adding particles to culture media was dependent on the MNP dosage, increasing with MNP concentration for both cell types. The iron content per cell reached a peak when the maximum concentration (100 μg/mL) of the as-prepared MNPs was used, with the iron loading being 14.24 pg/cell for Fb and 23.44 pg/cell for ADSCs. The coating significantly decreases the amount of iron/cell in both Fb and ADSCs at 14 and 28 days, respectively, for 20 and 40 μg/mL MNP concentrations, with the lowest amount recorded for OA-MNPs in Fb cells, while being only slightly decreased for 100 μg/mL for all MNP types after 28 days for Fb and for all MNPs types except PA-MNPs in ADSCs after 14 and 28 days (Figure 4a,b). Remarkably, while in Fb, the iron content/cell increases as a function of time, ADSCs internalize MNPs and retain a comparable amount of iron at 14 and 28 days for the as-prepared and OA-coated MNPs, while the PA-MNPs content increases with time.

Cell Senescence. We investigated the presence of beta-galactosidase, commonly associated with cellular senescence, by detecting its presence within cell culture (by ICC) and cellular lysates (by western blot) as well as by assessing enzyme functional activity using fluorometric FDG assay. As expected, cell beta-galactosidase activity increased with time in culture. We could detect that in the presence of MNPs, both the as-prepared and coated beta-galactosidase activity decreased but non-significantly, compared to nontreated controls in both ADSCs

https://doi.org/10.1021/acsomega.3c02449
ACS Omega 2023, 8, 23953−23963

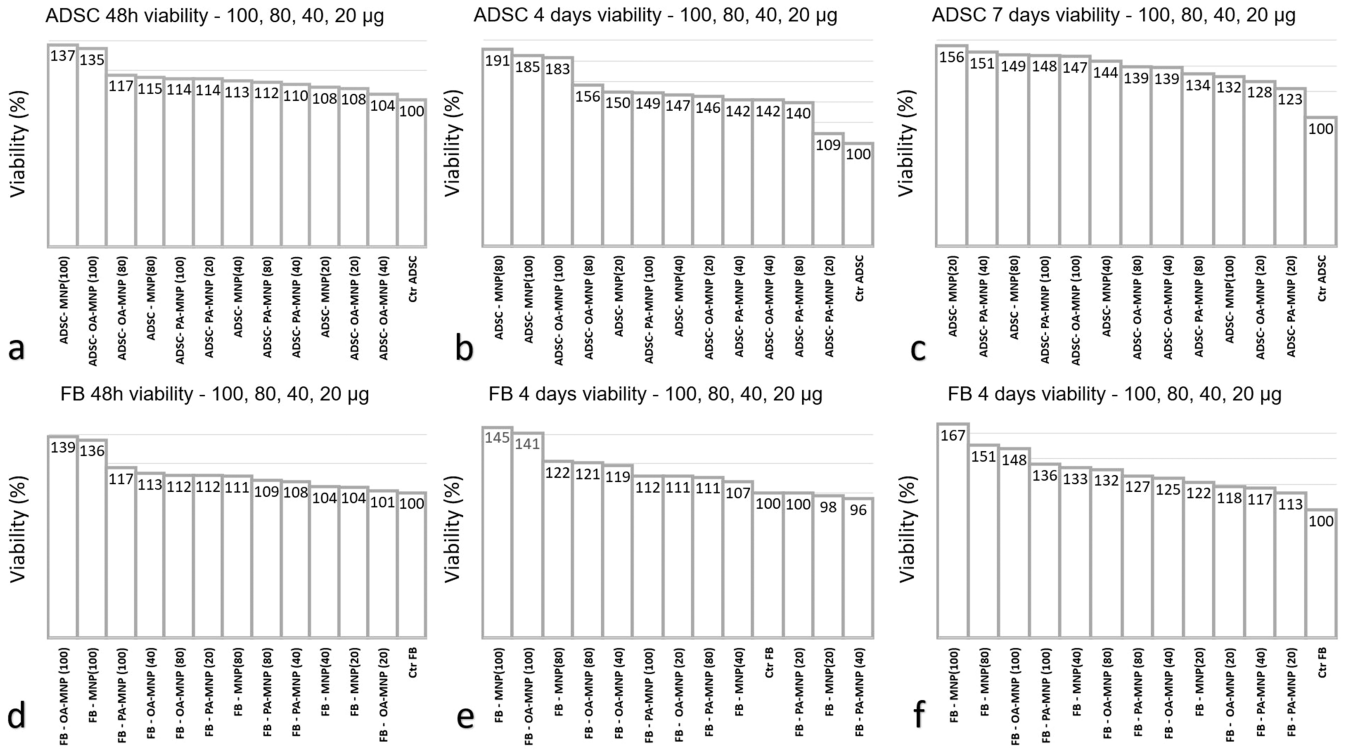

Figure 3. Cell viability (MTT assay) for adipose-derived stem cells (ADSCs) at (a) 48 h, (b) 4 days, and (c) 7 days for increasing concentrations of particles added in the culture media (20, 40, and 100 μg/mL). Cell viability (MTT assay) for fibroblasts (Fb) at (d) 48 h, (e) 4 days, and (f) 7 days for increasing concentrations of particles added in the culture media (20, 40, and 100 μg/mL). Fb = normal human dermal fibroblasts; ADSC = adipose-derived mesenchymal cells; percentual cell viability calculated in reference to nontreated controls for each cell type. MNP = magnetic nanoparticles; OA-MNPs = oleic acid-coated magnetic nanoparticles; and PA-MNPs = palmitic acid-coated nanoparticles.

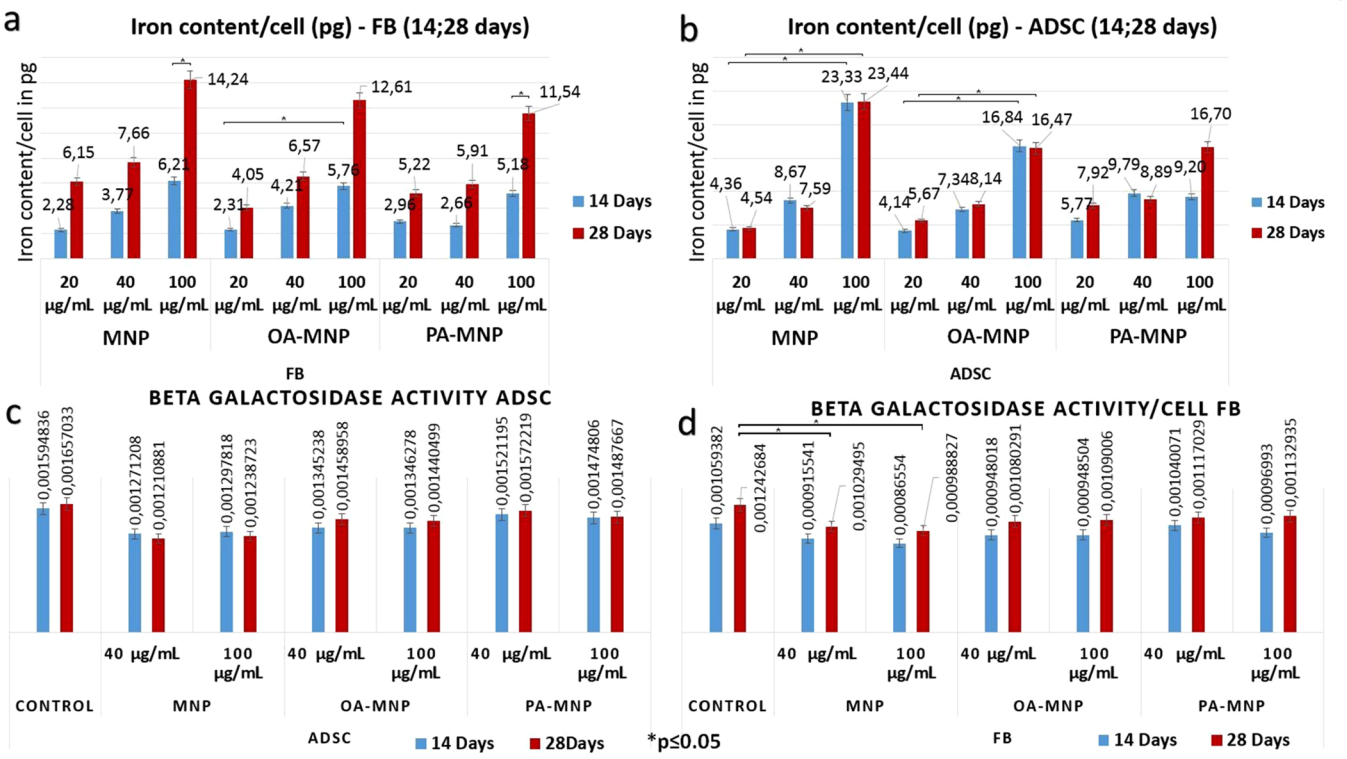

Figure 4. Iron content per cellular element detected using ferrozine assay at 14 and 28 days, respectively: (a) fibroblasts and (b) ADSCs. Enzymatic activity of beta-galactosidase detected using fluorometric assay (B-gal): (c) fibroblasts and (d) ADSC. MNPs = magnetic nanoparticles; OA-MNPs = oleic acid-coated magnetic nanoparticles; PA-MNPs = palmitic acid-coated nanoparticles; and * = significance bars for $p \leq 0.05$.

https://doi.org/10.1021/acsomega.3c02449
ACS Omega 2023, 8, 23953−23963

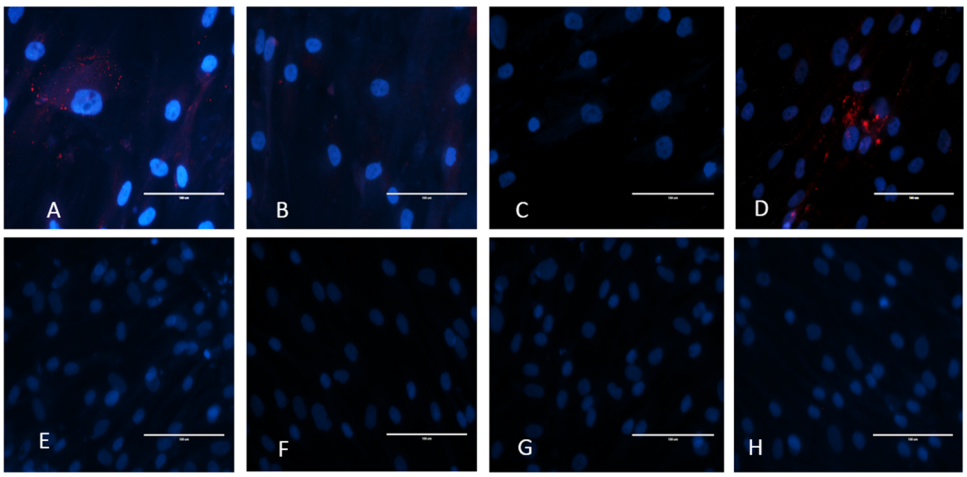

Figure 5. Immunocytochemistry staining for beta-galactosidase (B-Gal): (A) ADSCs: (B) ADSC-MNPs; (C) ADSC-OA-MNPs; (D) ADSC-PA-MNPs; (E) Fb; (F) Fb-MNPs; (G) Fb-OA-MNPs; and (H) Fb-PA-MNPs; ADSCs: adipose-derived mesenchymal stem cells; Fb: fibroblasts; MNPs = as-prepared magnetic nanoparticles; OA-MNPs: oleic acid-coated MNPs; PA-MNPs: palmitic acid-coated MNPs. Fluorescence images EVOS life imaging at 20× magnification; cell nuclei stained in blue (DAPI). Each photo represents the overlay of three pictures in red fluorescence, blue fluorescence (DAPI), and bright field microscopy.

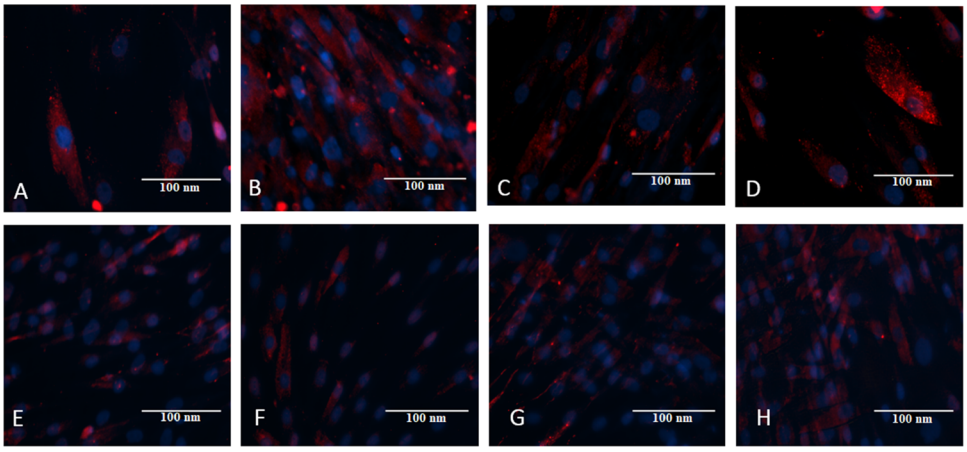

Figure 6. Immunocytochemistry staining for CXCR4: (A) ADSCs; (B) ADSC-MNPs; (C) ADSC-OA-MNPs; (D) ADSC-PA-MNPs; (E) Fb; (F) Fb-MNPs; (G) Fb-OA-MNPs; and (H) Fb-PA-MNPs. ADSCs: adipose-derived mesenchymal stem cells; Fb: fibroblasts; MNPs: as-prepared magnetic nanoparticles; OA-MNPs: oleic acid-coated MNPs; and PA-MNPs: palmitic acid-coated MNPs. Fluorescence images EVOS life imaging at 20× magnification; cell nuclei stained in blue (DAPI).

and Fb (Figure 4a,b). The only situation of a significant decrease compared to nontreated controls was observed for ADSC-MNPs (Figure 4a). Notably, for 40 μg/mL as well as 100 μg/mL MNP concentrations, enzyme activity after 28 days was slightly, nonsignificantly decreased compared to day 14 for ADSCs. Contrarily, in Fb, enzymatic beta-galactosidase activity was not influenced by the MNPs type or presence since similar enzymatic activity was recorded for controls and MNPs-treated Fb, slightly increasing at 28 days compared to 14 days.

Similar results were observed qualitatively by detecting beta-galactosidase at the protein level by immunocytochemistry and western blot. ADSCs apparently have an increased presence of beta-galactosidase compared to ADSC-MNPs and to ADSC-OA MNPs (Figure 5a−d).

Positive staining for beta-galactosidase could be observed in ADSC-PA MNPs. No positive staining could be detected by ICC in MNPs-loaded and nonloaded Fb at 14 days (Figure 5e−h). However, WB detected its presence within all investigated samples (Figure 7a).

Expression of CXCR4 and In Vitro Cell Mobility. The presence of the CXCR4 surface receptor was detected at the protein level using immunocytochemistry and western blot analysis. We found that CXCR4 is apparently more increased in ADSC-MNPs than in ADSC-PA-MNPs and OA-MNPs and controls (Figures 6a−d and 7b) as well as in Fb-MNPs compared to Fb-OA-MNPs and PA-MNPs and controls (Figures 6e−h and 7b).

Since CXCR4 is commonly considered a marker of increased mobility and targeting potential, we tested the cell ability to mobilize within a culture dish using a modified in vitro wound healing test and life imaging over 24 h. Images were taken at 10 min intervals in order to minimize the effect of light exposure on cells. We found that Fb as well as ADSCs displayed increased travel distance relative to time unit compared to their nonloaded counterparts; the effect was enhanced in the case of the as-prepared MNPs (Figure 7b,c).

We previously reported on the excellent biocompatibility of the as-prepared proprietary MNPs in relation to several mesenchymal stem cell types. Particularly, ADSCs were found

https://doi.org/10.1021/acsomega.3c02449
ACS Omega 2023, 8, 23953−23963

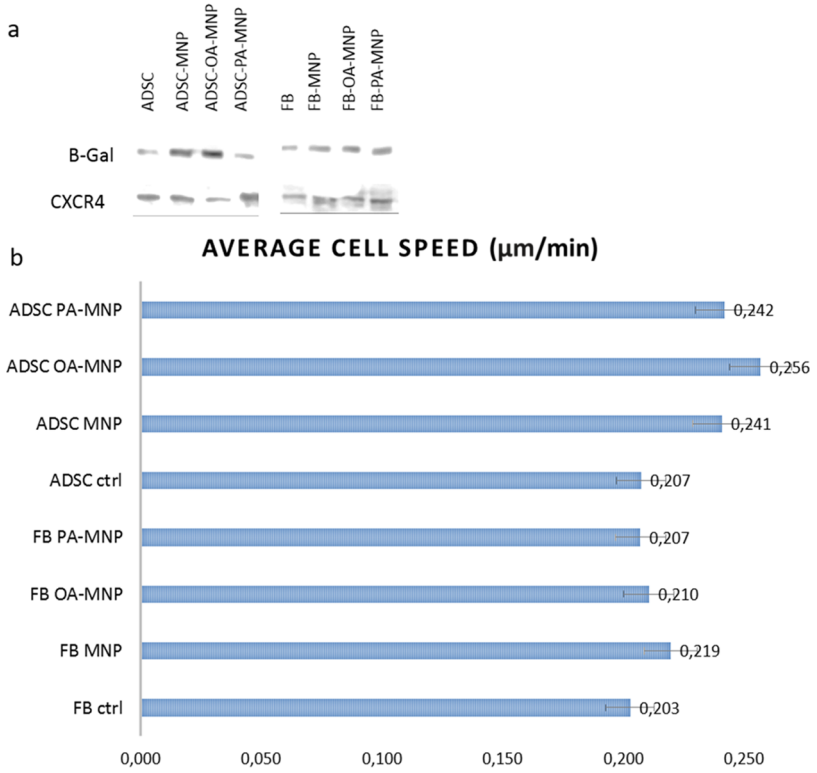

Figure 7. Western blot for (a) beta-galactosidase and (b) CXCR4 in Fb and ADSCs loaded with MNPs, OA-MNPs, and PA-MNPs. (b) Cell mobility as expressed by the individual cell element speed calculated as the distance traveled/minute as detected using 24 h life imaging in a "scratch" model of in vitro wound healing.

to retain the characteristic phenotype in terms of proliferation and three mesenchymal lineage differentiations.[15] For biological applications, various coatings are used as a modality to improve MNPs dispersity and colloidal stability and to delay particle degradation. Moreover, coatings are used as a modality to mediate MNPs functionalization with various drugs and/or bioactive molecules for the purpose of targeted delivery.[16] Note that all the 55 clinically available MNP-based agents currently used mostly as MRI tracers as well as subjects of undergoing clinical trials for various applications consist of polymer-coated MNPs.[17] Here, we compared proprietary MNPs coated with palmitic acid or oleic acid to discern the best choice in terms of viability, antisenescence, and expression of markers involved in targeting for two types of mesenchymal cells: normal dermal fibroblasts and primary ADSCs.

OA-coated MNPs have been reported to be water-dispersible, capable of binding different functional groups (such as carboxylic acid, amine, thiol), and remarkably stable in relation to human plasma, serum, and blood.[18] PA is one of the most common long-chain fatty acids used for coating MNPs due to its biocompatibility, high hydrophobic drug capsulation capability, and possibility for controlled release of drugs using triggers such as local hyperthermia.[19] We and other groups have previously reported on good viability and increased mesenchymal cell proliferation in the presence of the as-prepared Fe_3O_4. Particle biodegradation previously demonstrated in mesenchymal stem cells[20] and the crucial role of iron homeostasis in entering the cell cycle[21] are possible explanations of these findings. Since the coatings delay iron availability, we tested comparatively the as-prepared and lipid-coated MNPs for possible effects on cell viability/proliferation. We found that even though the as-prepared MNPs best support Fb and ADSC viability and proliferation, OA-MNP induces comparable (only slightly decreased) viability rates at all time points investigated even at high concentrations added in culture media (100 μg/mL). Both Fb and ADSCs exposed to PA-MNP tend to display decreased viability, albeit nonsignificant, after 4 days of cell−particle interaction (Figure 3), slightly increasing after 7 days. Such behavior can be explained by OA-MNP stability and possibly by the facilitated interaction with the outer layer of the cellular membrane. Indeed, endosome formation after foreign body uptake by cells is known to be dependent of the "protein corona", the modality in which MNPs "present" themselves to cells.[22] Formation of the protein corona in contact with serum in cell culture media has been reported to be largely influenced by nanoparticle coating, with PA increasing its homogeneity.[23] Nonprofessional phagocytic cells such as fibroblasts or ADSCs can engulf MNP complexes through phagocytosis, an opsonization-dependent process reported to be facilitated by fatty acids.[24]

The profile of iron load/cell seems to confirm the superior ability of ADSCs to incorporate MNPs. As expected, the iron content per cell is higher in the situation when an increased amount of MNPs is added in culture media. However, ADSCs accumulate a significant amount of iron compared to Fb for all particle types, which is increased but nonsignificantly higher, for the as-prepared sample compared to both OA and PA-MNP. All types of particle upload by ADSCs take place faster with a comparable amount of iron/cell detected at 14 and 28 days. Previous reports indicate the ADSC ability to uptake the maximum amount of iron even from the first 24 h in culture.[15,20] We found that even though lipid coating decreases the amount of particle upload, it does not slow the process as comparable amounts could be retrieved in ADSCs exposed to the as-

https://doi.org/10.1021/acsomega.3c02449
ACS Omega 2023, 8, 23953−23963

prepared and coated MNPs. The maximum iron/cell accumulated by ADSCs for both OA- and PA-coated samples remains within the range that endows cells with responsivity to an applied magnetic field, which are therefore detectable using MRI[25] or magnetic particle imaging.[26] Fibroblasts were found to be slower to accumulate all types of MNPs we tested, which takes place in lower amounts. This can be explained by one side by the fact that they are only occasionally phagocytic cells as well as by the fact that cellular bodies are smaller compared to ADSCs in two-dimensional culture and therefore able to incorporate lower amounts of foreign materials. Such differences in the functional ability of fibroblasts compared to adipose tissue-derived progenitors have been previously reported.[27] Their reduced ability to uptake and store iron needs to be taken into account when designing MNP-based local or regional delivery of bioactive compounds.

We then investigated the effect of MNP uptake on culture-induced senescence, focusing on identifying the presence of a commonly used marker, B-Gal, at the protein level in medium- and long-term cultured ADSCs and fibroblasts loaded with MNPs. Our previous results pointed out that ADSCs, but not Wharton jelly mesenchymal stem cells, loaded with the as-prepared MNPs, express lower B-Gal activity at 28 days in continuous culture, suggesting that this effect might be cell-dependent.

The B-Gal presence could be identified by WB in ADSCs cultured for 14 days. We confirmed the presence of B-Gal at the protein level using ICC, which is apparently higher in ADSCs compared to ADSC-MNP but not to ADSC-OA-MNP. The lack of fluorescence signals in fibroblasts in ICC staining for B-Gal can be possibly explained by differences in antibody permeability for this cell type. WB, however, confirmed the presence of B-Gal at 14 days in both fibroblasts and ADSCs loaded or nonloaded with MNPs.

Since B-Gal lysosomal accumulation does not obligatorily parallel its functionality,[28] we further investigated enzymatic activity using fluorescence quantitation. We found that only the as-prepared MNPs significantly decreased enzyme activity at 28 days and both OA- and PA-coated MNPs do decrease B-Gal compared to nonloaded ADSCs but nonsignificantly with PA-MNP inducing slightly lower levels. This effect has not been reproduced in fibroblasts, which do not seem to experience a significant decrease in enzyme activity with any type of MNPs, expressing, however, lower, albeit nonsignificant, values in the presence of all three MNP variants used in the experiment. Further tests are needed to detect the cause of decreased senescence induced by bare MNPs only at the molecular level. One possible explanation can be the different rates of endolysosomal trafficking and particle degradation previously found to be affected by the MNP coating as well as cell type.[29] It is presumable that bare MNP lysosomal uptake results in more rapid particle degradation and consequently cytosolic ferritin content as well as reactive oxygen species (ROS) balance. The hormetic role of ROS in influencing the cellular homeostatic mechanism could result in decreased beta-galactosidase enzyme activation.[30] Senescent cells were found to contain ferroportin predominantly localized to an intracellular compartment and not at the plasma membrane.[31] MNP uptake by mesenchymal stem cells increased the expression of the iron exporter ferroportin and iron-storing ferritin, a process that is cell type-dependent and fine-tuned. It is possible that this activation counteracts culture-induced senescence, a fact that needs further investigation.

We next tested the presence of the chemokine receptor CXCR4, a surface membrane commonly involved in mesenchymal cell and stem cell mobility and targeting abilities. The SDF-1/CXCR4 axis is known to represent one of the major factors regulating migration and homing for mesenchymal progenitors.[32] Increasing the CXCR4 expression in ADSCs regionally or systemically delivered regenerative cell therapy.[33] Various groups are testing methods for engineering MSCs to overexpress CXCR4 to improve their targeting abilities.[34,35] Few previous observations suggest that iron nanoclusters consisting of zinc-doped iron oxide ($Zn_{0.4}Fe_{2.6}O_4$) and amphiphilic polymers increase the expression of CXCR4 in bone marrow MSCs as well as their targeting abilities.[36] Here, we found reasons to interpret that MNP-loaded ADSCs display increased CXCR4 compared to nonloaded cells based on its detection by ICC and WB. Since the methods we used here are not quantitative, we further tested the cell migratory ability in an in vitro model of wound healing, the "scratch assay".[37] The purpose was to verify if the apparently increased CXCR4 presence we previously detected translates into functional cellular motility. We found that the average speed calculated as the distance traveled within the culture dish by individual cell elements per 24 h increased in MNP-loaded Fb and ADSCs compared to controls. A significant increase of cell speed could be detected in the case of ADSC-OA-MNP compared to controls (Figure 7b). Only a moderate increase could be observed in the case of OA- and PA-MNP-loaded cells compared to nonloaded controls. Not surprisingly, we found that ADSCs tend to have increased mobility compared to Fb; however, it is nonsignificant. MSCs have been described to possess phenotypic features of putative migratory elements involved in tissue reparative processes. ADSCs in particular were shown to target sites of injury, inflammation, or tumor, displaying higher mobility upon stimulation.[38] Dermal fibroblasts have the ability to initiate migration both in vitro and in vivo during wound healing.[39] Here, we found that the MNP upload can increase the cell type mobility in the model created, particularly in the case of the OA coating. Different strategies of MSC preconditioning using physical or biochemical stimuli have been used to increase their migratory and targeting potential; small molecules, hypoxia, or metal salts have been tested as methods of MSC preconditioning.[40] Copper preconditioning was found to increase ADSC migration by Cu stimulating phosphorylation of vimentin Ser39.[41] In another study, Zinc nanoparticle upload was shown to increase the cytoskeletal fiber dynamics in a YAP-TAZ-dependent mechanism.[42] It is possible that MNP internalization and trafficking increase cytoskeletal dynamics of ADSCs loaded with MNPs, enhancing the migratory ability, an effect potentially slightly accentuated in the case of OA-coated MNPs due to their colloidal stability. We can speculate that cytoskeletal dynamics normally activated during mesenchymal cell mobilization required for tissue repair and wound healing could be a priori induced by the cellular processes of MNPs upload and intracellular trafficking. This could result in an "activated" cellular phenotype more prone to execute tissue reparative processes.

While further studies are needed to confirm this observation *in vivo*, we show that the MNPs upload can act as a modality of preconditioning ADSCs for increasing resistance to culture-induced senescence during the in vitro expansion for potential cell therapies and for inducing an increased expression of cell surface markers involved in targeting and migration. Since every

https://doi.org/10.1021/acsomega.3c02449
ACS Omega 2023, 8, 23953−23963

potential therapeutic use of cell therapy requires complete characterization, in-depth proteomic studies would be needed before embarking in a chosen therapeutic scenario.

Furthermore, our findings are of importance in choosing the type of MNPs coating for a particular cell therapy application. The use of cells loaded with OA-coated MNPs would benefit wound healing or organ targeting aimed to enhance reparative processes such as myocardial infarction[43] or kidney failure.[44]

CONCLUSIONS

To the best of our knowledge, this is the first report on comparative evaluation of coating types related to mesenchymal stem cells in terms of senescence and mobility in vitro. We found that the as-prepared and OA-coated iron oxide MNPs account for significantly increased cell viability up to 7 days, while PA-MNP viability increases nonsignificantly. A significant decrease in senescence-associated B-Gal activity could be detected only in the presence of the as-prepared MNPs only in ADSCs. Remarkably, OA-MNP upload significantly increases ADSC mobility in a wound healing model in vitro compared to nonloaded counterparts. These observations need to be validated in vivo. However, the present findings pave the way for potential applications of OA-MNP in wound healing and cell therapy involving reparative processes.

ASSOCIATED CONTENT

Supporting Information

The Supporting Information is available free of charge at https://pubs.acs.org/doi/10.1021/acsomega.3c02449.

Proliferative potential of ADSCs calculated as PD = (LOG($p1$) − LOG(p))/LOG(2) (PDF)

AUTHOR INFORMATION

Corresponding Authors

Luminiţa Lăbuscă − *Department of Magnetic Materials and Devices, National Institute of Research and Development for Technical Physics, 700050 Iaşi, Romania; County Emergency Hospital Saint Spiridon, Orthopedics and Traumatology Clinic, 700111 Iaşi, Romania;* orcid.org/0000-0001-9635-6893; Email: drlluminita@yahoo.com

Dumitru-Daniel Herea − *Department of Magnetic Materials and Devices, National Institute of Research and Development for Technical Physics, 700050 Iaşi, Romania;* orcid.org/0000-0002-8455-8380; Email: dherea@phys-iasi.ro

Authors

Camelia-Mihaela Zară-Dănceanu − *Department of Magnetic Materials and Devices, National Institute of Research and Development for Technical Physics, 700050 Iaşi, Romania;* orcid.org/0000-0002-3400-2421

Anca-Emanuela Minuti − *Department of Magnetic Materials and Devices, National Institute of Research and Development for Technical Physics, 700050 Iaşi, Romania; Faculty of Physics, Alexandru Ioan Cuza University, 700506 Iaşi, Romania;* orcid.org/0009-0005-4319-2545

Cristina Stavilă − *Department of Magnetic Materials and Devices, National Institute of Research and Development for Technical Physics, 700050 Iaşi, Romania; Faculty of Physics, Alexandru Ioan Cuza University, 700506 Iaşi, Romania;* orcid.org/0009-0002-5719-710X

Crina Elena Tiron − *Regional Institute of Oncology, 700483 Iaşi, Romania*

Horia Chiriac − *Department of Magnetic Materials and Devices, National Institute of Research and Development for Technical Physics, 700050 Iaşi, Romania*

Nicoleta Lupu − *Department of Magnetic Materials and Devices, National Institute of Research and Development for Technical Physics, 700050 Iaşi, Romania;* orcid.org/0000-0003-2188-8187

Complete contact information is available at: https://pubs.acs.org/10.1021/acsomega.3c02449

Author Contributions

⊥C.-M.Z.-D. and A.-E.M. contributed equally to this work.

Notes

The authors declare no competing financial interest.

ACKNOWLEDGMENTS

Financial support by Romanian Ministry of Research, Innovation and Digitization, CNCS/CCCDI-UEFISCDI, project number ERANET-EURONANOMED-3-OASIs, within PNCDI III (contract no. 273/2022) is kindly acknowledged.

REFERENCES

(1) Anderson, S. D.; Gwenin, V. V.; Gwenin, C. D. Magnetic Functionalized Nanoparticles for Biomedical, Drug Delivery and Imaging Applications. *Nanoscale Res Lett.* **2019**, *14*, 1−16.

(2) Chen, Y.; Hou, S. Application of magnetic nanoparticles in cell therapy. *Stem Cell Res. Ther.* **2022**, *13*, No. 135.

(3) Daya, R.; Changlu, X.; Nhu-Y, T. N.; Huinan, H. L. Angiogenic Hyaluronic Acid Hydrogels with Curcumin-Coated Magnetic Nanoparticles for Tissue Repair. *ACS Appl. Mater. Interfaces* **2022**, *14*, 11051−11067.

(4) Zhang, C.; Cai, Y. Z.; Lin, X. J.; Wang, Y. Magnetically Actuated Manipulation and Its Applications for Cartilage Defects: Characteristics and Advanced Therapeutic Strategies. *Front. Cell Dev. Biol.* **2020**, *8*, No. 526.

(5) Perea, H.; Aigner, J.; Heverhagen, J. T.; Hopfner, U.; Wintermantel, E. Vascular tissue engineering with magnetic nanoparticles: seeing deeper. *J. Tissue Eng. Regener. Med.* **2007**, *1*, 318−321.

(6) Lee, E. A.; Yim, H.; Heo, J.; Kim, H.; Jung, G.; Hwang, N. S. Application of magnetic nanoparticle for controlled tissue assembly and tissue engineering. *Arch. Pharm. Res.* **2014**, *37*, 120−128.

(7) Włodarczyk, A.; Gorgoń, S.; Radoń, A.; Bajdak-Rusinek, K. Magnetite Nanoparticles in Magnetic Hyperthermia and Cancer Therapies: Challenges and Perspectives. *Nanomaterials* **2022**, *12*, 1807.

(8) Levy, M.; Luciani, N.; Alloyeau, D.; Elgrabli, D.; Deveaux, V.; Pechoux, C.; Chat, S.; Wang, G.; Vats, N.; Gendron, F.; Factor, C.; Lotersztajn, S.; Luciani, A.; Wilhelm, C.; Gazeau, F. Long term in vivo biotransformation of iron oxide nanoparticles. *Biomaterials* **2011**, *32*, 3988−3999.

(9) Abakumov, M. A.; Semkina, A. S.; Skorikov, A. S.; Vishnevskiy, D. A.; Ivanova, A. V.; Mironova, E.; Davydova, G. A.; Majouga, A. G.; Chekhonin, V. P. Toxicity of iron oxide nanoparticles: Size and coating effects. *J. Biochem. Mol. Toxicol.* **2018**, *32*, No. e22225.

(10) Mohsin, A.; Hussain, M. H.; Mohsin, M. Z.; Zaman, W. Q.; et al. Recent Advances of Magnetic Nanomaterials for Bioimaging, Drug Delivery, and Cell Therapy. *ACS Appl. Nano Mater.* **2022**, *8*, 10118−10136.

(11) Micheletti, G.; Boga, C.; Telese, D.; et al. Magnetic Nanoparticles Coated with (R)-9-Acetoxystearic Acid for Biomedical Applications. *ACS Omega* **2020**, *5*, 12707−12715.

(12) Labusca, L.; Herea, D. D.; Minuti, E. A.; Stavila, C.; Danceanu, C.; Plamadeala, P.; Chiriac, H.; Lupu, N. Magnetic Nanoparticles and Magnetic Field Exposure Enhances Chondrogenesis of Human Adipose Derived Mesenchymal Stem Cells but Not of Wharton Jelly Mesenchymal Stem Cells. *Front Bioeng. Biotechnol.* **2021**, *9*, No. 737132.

(13) Zuk, P. A.; Zhu, M.; Ashjian, P.; De Ugarte, D. A.; Huang, J. I.; Mizuno, H.; Alfonso, Z. C.; Fraser, J. K.; Benhaim, P.; Hedrick, M. H. Human adipose tissue is a source of multipotent stem cells. *Mol. Biol. Cell* **2002**, *13*, 4279−4295.
(14) Henrot, P.; Laurent, P.; Levionnois, E.; Leleu, D.; Pain, C.; Truchetet, M. E.; Cario, M. A Method for Isolating and Culturing Skin Cells: Application to Endothelial Cells, Fibroblasts, Keratinocytes, and Melanocytes from Punch Biopsies in Systemic Sclerosis Skin. *Front. Immunol.* **2020**, *11*, No. 566607.
(15) Labusca, L.; Herea, D. D.; Minuti, A. E.; Stavila, C.; Danceanu, C.; Grigoras, M.; Ababei, G.; Chiriac, H.; Lupu, N. Magnetic nanoparticle loaded human adipose derived mesenchymal cells spheroids in levitated culture. *J. Biomed. Mater. Res., Part B.* **2021**, *109*, 630−642.
(16) Subbiah, R.; Veerapandian, M.; Yun, K. S. Nanoparticles: functionalization and multifunctional applications in biomedical sciences. *Curr. Med. Chem.* **2010**, *17*, 4559−4577.
(17) Bobo, D.; Robinson, K. J.; Islam, J.; Thurecht, K. J.; Corrie, S. R. Nanoparticle-Based Medicines: A Review of FDA-Approved Materials and Clinical Trials to Date. *Pharm Res.* **2016**, *33*, 2373−2387.
(18) Bloemen, M.; Brullot, W.; Luong, T. T.; Geukens, N.; Gils, A.; Verbiest, T. Improved functionalization of oleic acid-coated iron oxide nanoparticles for biomedical applications. *J. Nanopart. Res.* **2012**, *14*, No. 1100.
(19) Kalaycioglu, G. D. Preparation of magnetic nanoparticle integrated nanostructured lipid carriers for controlled delivery of ascorbyl palmitate. *MethodsX* **2020**, *7*, No. 101147.
(20) Van de Walle, A.; Plan Sangnier, A.; Abou-Hassan, A.; Curcio, A.; Hémadi, M.; Menguy, N.; Lalatonne, Y.; Luciani, N.; Wilhelm, C. Biosynthesis of magnetic nanoparticles from nano-degradation products revealed in human stem cells. *Proc. Natl. Acad. Sci. U.S.A.* **2019**, *116*, 4044−4053.
(21) Weber, R. A.; Yen, F. S.; Nicholson, S.P.V.; Alwaseem, H.; Bayraktar, E. C.; Alam, M.; Timson, R. C.; La, K.; Abu-Remaileh, M.; Molina, H.; Birsoy, K. Maintaining Iron Homeostasis Is the Key Role of Lysosomal Acidity for Cell Proliferation. *Mol. Cell.* **2020**, *77*, 645−655.
(22) Sousa de Almeida, M.; Susnik, E.; Drasler, B.; Taladriz-Blanco, P.; Petri-Fink, A.; Rothen-Rutishauser, B. Understanding nanoparticle endocytosis to improve targeting strategies in nanomedicine. *Chem. Soc. Rev.* **2021**, *50*, 5397−5434.
(23) Abesekara, M. S.; Chau, Y. Recent advances in surface modification of micro- and nano-scale biomaterials with biological membranes and biomolecules. *Front. Bioeng. Biotechnol.* **2022**, *10*, No. 972790.
(24) Madore, C.; Leyrolle, Q.; Morel, L.; Rossitto, M.; Greenhalgh, A. D.; Delpech, J. C.; Martinat, M.; Bosch-Bouju, C.; Bourel, J.; Rani, B.; Lacabanne, C.; Thomazeau, A.; Hopperton, K. E.; Beccari, S.; Sere, A.; Aubert, A.; De Smedt-Peyrusse, V.; Lecours, C.; Bisht, K.; Fourgeaud, L.; Gregoire, S.; Bretillon, L.; Acar, N.; Grant, N. J.; Badaut, J.; Gressens, P.; Sierra, A.; Butovsky, O.; Tremblay, M. E.; Bazinet, R. P.; Joffre, C.; Nadjar, A.; Layé, S. Essential omega-3 fatty acids tune microglial phagocytosis of synaptic elements in the mouse developing brain. *Nat. Commun.* **2020**, *11*, No. 6133.
(25) Liu, W.; Frank, J. A. Detection and quantification of magnetically labeled cells by cellular MRI. *Eur. J. Radiol.* **2009**, *70*, 258−264.
(26) Sehl, O. C.; Gevaert, J. J.; Melo, K. P.; Knier, N. N.; Foster, P. J. A Perspective on Cell Tracking with Magnetic Particle Imaging. *Tomography* **2020**, *6*, 315−324.
(27) Brohem, C. A.; de Carvalho, C. M.; Radoski, C. L.; Santi, F. C.; Baptista, M. C.; Swinka, B. B.; de A Urban, C.; de Araujo, L. R. R.; Graf, R. M.; Feferman, I. H. S.; Lorencini, M. Comparison between fibroblasts and mesenchymal stem cells derived from dermal and adipose tissue. *Int. J. Cosmet Sci.* **2013**, *35*, 448−457.
(28) Lee, B. Y.; Han, J. A.; Im, J. S.; Morrone, A.; Johung, K.; Goodwin, E. C.; Kleijer, W. J.; Di Maio, D.; Hwang, E. S. Senescence-associated beta-galactosidase is lysosomal beta-galactosidase. *Aging Cell* **2006**, *5*, 187−195.
(29) Portilla, Y.; Mulens-Arias, V.; Paradela, A.; Ramos-Fernández, A.; Pérez-Yagüe, S.; Morales, M. P.; Barber, D. F. The surface coating of iron oxide nanoparticles drives their intracellular trafficking and degradation in endolysosomes differently depending on the cell type. *Biomaterials* **2022**, *281*, No. 121365.
(30) Ludovico, P.; Burhans, W. C. Reactive oxygen species, ageing and the hormesis police. *FEMS Yeast Res.* **2014**, *14*, 33−39.
(31) Masaldan, S.; Clatworthy, S. A. S.; Gamell, C.; Meggyesy, P. M.; Rigopoulos, A. T.; Haupt, S.; Haupt, Y.; Denoyer, D.; Adlard, P. A.; Bush, A. I.; Cater, M. A. Iron accumulation in senescent cells is coupled with impaired ferritinophagy and inhibition of ferroptosis. *Redox Biol.* **2018**, *14*, 100−115.
(32) Zhang, H.; Li, X.; Li, J.; Zhong, L.; Chen, X.; Chen, S. SDF-1 mediates mesenchymal stem cell recruitment and migration via the SDF-1/CXCR4 axis in bone defect. *J. Bone Miner. Metab.* **2021**, *39*, 126−138.
(33) Ma, H. C.; Shi, X. L.; Ren, H. Z.; Yuan, X. W.; Ding, Y. T. Targeted migration of mesenchymal stem cells modified with CXCR4 to acute failing liver improves liver regeneration. *World J. Gastroenterol.* **2014**, *20*, 14884−14894.
(34) Kalimuthu, S.; Oh, J. M.; Gangadaran, P.; Zhu, L.; Lee, H. W.; Rajendran, R. L.; Baek, S. H.; Jeon, Y. H.; Jeong, S. Y.; Lee, S. W.; Lee, J.; Ahn, B. C. In Vivo Tracking of Chemokine Receptor CXCR4-Engineered Mesenchymal Stem Cell Migration by Optical Molecular Imaging. *Stem Cells Int.* **2017**, *2017*, No. 8085637.
(35) Cheng, Z.; Ou, L.; Zhou, X.; Li, F.; Jia, X.; Zhang, Y.; Liu, X.; Li, Y.; Ward, C. A.; Melo, L. G.; Kong, D. Targeted migration of mesenchymal stem cells modified with CXCR4 gene to infarcted myocardium improves cardiac performance. *Mol. Ther.* **2008**, *16*, 571−579.
(36) Huang, X.; Zhang, F.; Wang, Y.; Sun, X.; Choi, K. Y.; Liu, D.; Choi, J. S.; Shin, T. H.; Cheon, J.; Niu, G.; Chen, X. Design considerations of iron-based nanoclusters for noninvasive tracking of mesenchymal stem cell homing. *ACS Nano.* **2014**, *8*, 4403−4414.
(37) Moulin, V.; Castilloux, G.; Jean, A.; Garrel, D. R.; Auger, F. A.; Germain, L. In vitro models to study wound healing fibroblasts. *Burns* **1996**, *22*, 359−362.
(38) Glenn, J. D.; Whartenby, K. A. Mesenchymal stem cells: Emerging mechanisms of immunomodulation and therapy. *World J. Stem Cells* **2014**, *6*, 526−539.
(39) Monsuur, H. N.; Boink, M. A.; Weijers, E. M.; Roffel, S.; Breetveld, M.; Gefen, A.; van den Broek, L. J.; Gibbs, S. Methods to study differences in cell mobility during skin wound healing in vitro. *J Biomech.* **2016**, *49*, 1381−1387.
(40) Yuan, X.; Li, L.; Liu, H.; et al. Strategies for improving adipose-derived stem cells for tissue regeneration. *Burns Trauma* **2022**, *10*, No. tkac028.
(41) Chen, M.; Li, R.; Yin, W.; Wang, T.; Kang, Y. J. Copper promotes migration of adipose-derived stem cells by enhancing vimentin-Ser39 phosphorylation. *Exp. Cell Res.* **2020**, *388*, No. 111859.
(42) Laiman, V.; Heriyanto, D. S.; Lee, Y.-L.; Lai, C.-H.; Pan, C.-H.; Chen, W.-L.; Wang, C.-C.; Chuang, K.-J.; Chang, J.-H.; Chuang, H.-C. Zinc Oxide Nanoparticles Promote YAP/TAZ Nuclear Localization in Alveolar Epithelial Type II Cells. *Atmosphere* **2022**, *13*, No. 334.
(43) Santoso, M. R.; Yang, P. C. Magnetic Nanoparticles for Targeting and Imaging of Stem Cells in Myocardial Infarction. *Stem Cells Int.* **2016**, *2016*, No. 4198790.
(44) Hauger, O.; Frost, E. E.; van Heeswijk, R.; Deminière, C.; Xue, R.; Delmas, Y.; Combe, C.; Moonen, C. T.; Grenier, N.; Bulte, J. W. MR evaluation of the glomerular homing of magnetically labeled mesenchymal stem cells in a rat model of nephropathy. *Radiology* **2006**, *238*, 200−210.

https://doi.org/10.1021/acsomega.3c02449
ACS Omega 2023, 8, 23953−23963